International Journal on Magnetic Particle Imaging
Vol 9, No 1, Suppl 1, Article ID 2303023, 4 Pages

Infinite Science Publishing

Proceedings Article

Flexible Selection Field Generation using Iron Core Coil Arrays

Fynn Foerger [1,2,*] · Niklas Hackelberg [1,2] · Marija Boberg [1,2] · Jan-Philipp Scheel [3,4] · Florian Thieben [1,2] · Liana Mirzojan [3,4] · Fabian Mohn [1,2] · Martin Möddel [1,2] · Matthias Graeser [1,2,3,4] · Tobias Knopp [1,2]

[1]Section for Biomedical Imaging, University Medical Center Hamburg-Eppendorf, Hamburg, Germany
[2]Institute for Biomedical Imaging, Hamburg University of Technology, Hamburg, Germany
[3]Fraunhofer Research Institute for Individualized and Cell-based Medicine, IMTE, Lübeck, Germany
[4]Institute for Medical Engineering, University of Lübeck, Lübeck, Germany
*Corresponding author, email: f.foerger@uke.de

Abstract

Many different concepts for selection-field generators have been introduced for Magnetic Particle Imaging so far. In this work, the field generation characteristics of an optimized iron core selection-field generator consisting of two coil arrays with a total of 18 coils are presented. Due to the high number of degrees of freedom, a wide variety of field configurations are possible. The setup allows the generation of arbitrarily shaped fields, including the standard Magnetic Particle Imaging fields such as field-free points and field-free lines. In this work, measurements of static magnetic fields are presented and the current calculation method for generating a specific field configuration is discussed.

I. Introduction

One of the main targets of current Magnetic Particle Imaging (MPI) research is its scaling and application to humans. An essential component of an MPI scanner is the magnetic field generator, which produces the selection field. Due to the selection field, the spatial encoding of the measurement signal is achieved. The selection field is a magnetic gradient field that accommodates a field-free region. Depending on the desired scanner topology, this is often realized by a field-free point (FFP) or a field-free line (FFL). When scanners are scaled up to human size, the power and cooling requirements of selection-field generators pose a major challenge. For this reason, a wide variety of magnetic field generators have been introduced in recent years [1–5]. Some use air coils, others permanent magnets or coils with iron cores, or combinations of the previous. Depending on the field generation strategy, there are different advantages and disadvantages. Especially when using soft iron, an optimization of the generator topology can make a significant difference in the overall power consumption.

In this work, magnetic field measurements of the field generator introduced in [6] are presented. It uses two sets of opposing coils with iron cores arranged in an array for field generation. During the design process, various parameters, such as the number and size of the coils and cores, were optimized. The setup is able to produce highly flexible static magnetic fields in an efficient way. It can generate FFPs, FFLs, as well as homogeneous fields. This allows applications such as imaging or magnetic manipulation with easy access to the operational field region. The main objective of this work is to show the field generation possibilities offered by the system.

10.18416/ijmpi.2023.2303023

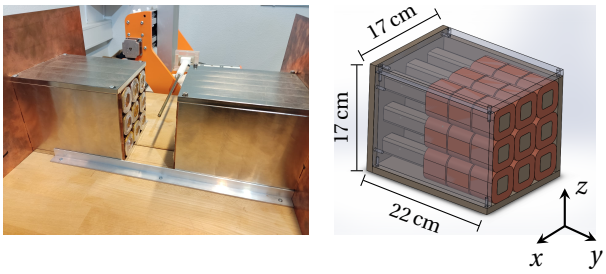

Figure 1: Photo of the field generator and schematic rendering of one coil cage. Each cage contains nine iron core coils placed in a housing made of 1 cm thick iron plates. On the left side, a 3D hall probe is moved by a robot to measure the field.

II. Methods

Besides the design and realization of the system, its operation requires methods to produce desired fields and to quantify the system.

II.I. The Field Generator

The field generator design and first measurements have already been presented [6]. The generator consists of a total of 18 iron core coils arranged in two opposing coil arrays with a distance of 10 cm, as shown in Figure 1. Each coil can be individually supplied with bipolar current. To avoid current disturbances due to coil coupling, all coils are equipped with an individual, custom analog PID controller that measures and adjusts the current. The controllers are tuned to switching frequencies of 10 Hz with a current amplitude of 30 A. [7] They receive their set value by a cluster of nine RedPitaya IO boards (STEMlab 125-14, RedPitaya, Solkan, Slovenia), which together with other devices, such as hall probes and a robot, are controlled by a software stack composed of our open-source software RedPitayaDAQServer [8] and MPIMeasurements.jl [9].

II.II. Current Calculation

The magnetic flux is generated by a controlled current density and its interaction with the inbuilt soft iron. One of the biggest challenges of the setup is to find the required currents for a desired field. Due to the nonlinear nature of the iron magnetization, this leads in general to a nonlinear inverse problem. However, as a first approximation, it is assumed that the fields of the coils depend linearly on their currents. In this scenario, coil sensitivities can be defined and the currents can be calculated similar to [4]. Depending on which entries of the Jacobian matrix are used at the considered position, different fields can be generated in this way. This method was used, for example, for the FFLs shown in Figure 2. In this case all field derivatives in one direction have to vanish.

This method is only applicable for small current densities, where saturation effects can be neglected. If the linear approach breaks down, it is useful to set up an optimization problem where the field requirements in terms of the field-free region position (4) and the field derivatives ((2),(3), here stated for an FFP) are given as constraints. The objective function of the optimization problem is then defined over the power consumption of the system:

$$\min_{I_k} \sum_{k=1}^{N} R_k I_k^2 \tag{1}$$

$$\text{s.t.} \quad \sigma_1 / g \geq 1 \tag{2}$$

$$\sigma_3 / \sigma_1 \geq \alpha \tag{3}$$

$$\rho_j \leq \beta, \quad \text{for } j \in \{x, y, z\}. \tag{4}$$

Here, the resistances and currents of the coils are denoted by R_k and I_k, respectively. σ_1 and σ_3 are the first and third singular values of the Jacobian matrix at the desired FFP position $\boldsymbol{x}_t$. g is a measure for the gradient strength. Depending on the choice of $\alpha > 0$, the field norm is forced to increase as homogeneously as possible such that no FFLs are created. Using the singular values instead of the explicit entries of the Jacobian matrix allows the optimization algorithm to rotate and shear the gradient field. ρ_j are the absolute values of the remaining offset field components at $\boldsymbol{x}_t$. For $\rho_j \leq \beta$ the FFP is near the target position and the remaining displacement is tolerable. Depending on the FFP position, this can result in a significant power reduction. The optimization was performed using the FEM software COMSOL Multiphysics[1] with a simplified model of the setup.

II.III. Field Quantification

Field measurements were performed using the measurement procedure presented in [10], providing polynomial expansions of the fields with a high accuracy while only few measurement points are required. To cope with the highly non-linear field profile generated by the iron core coils, a spherical 12-design with 86 measurement points on a sphere with a radius of 4 cm was chosen, which provides polynomials of degree 6 describing the magnetic fields. Additionally, the field's expansion can be used to easily calculate all field derivatives at any position. At every sampling position, constant fields of 250 ms duration are applied during field measurements.

III. Results

Figure 2 shows different field configurations. Besides the generation of FFPs, for which the setup was originally optimized, FFLs can also be generated. Depending on

[1] COMSOL Multiphysics® v. 5.6. www.comsol.com. COMSOL AB, Stockholm, Sweden.

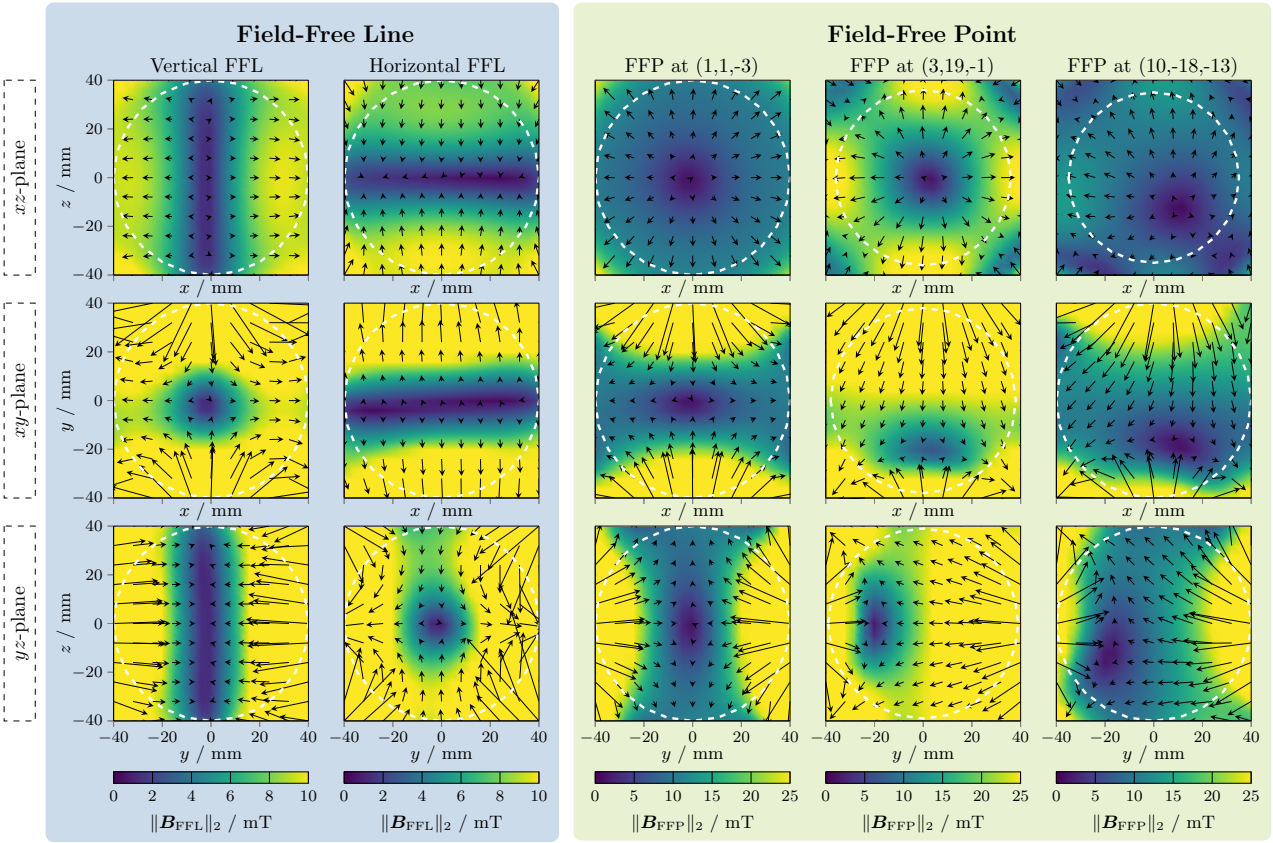

Figure 2: Measurement of generated magnetic fields. Each column shows a different field, including FFL (left) and FFP (right) fields, with sections of different planes shown in each row. The white dotted circle indicates the sphere on which the measured values were taken. Outside this circle, the field values cannot be trusted. For the FFLs it holds that $\sigma_1 = \sigma_2 = 0.5\,\mathrm{T\,m^{-1}}$ and $\sigma_3 \leq 0.025\,\mathrm{T\,m^{-1}}$. The first FFP has a central position with $\sigma_1 = 1.0\,\mathrm{T\,m^{-1}}$, $\sigma_3 = 0.5\,\mathrm{T\,m^{-1}}$. The second FFP is shifted by 2 cm towards the coil cages. At this position $\sigma_1 = 1.8\,\mathrm{T\,m^{-1}}$, $\sigma_3 = 0.7\,\mathrm{T\,m^{-1}}$ was achievable. At the third FFP position $\sigma_1 = 0.8\,\mathrm{T\,m^{-1}}$, $\sigma_3 = 0.3\,\mathrm{T\,m^{-1}}$ are measured.

the FFP and FFL position, different field gradients are achievable. In the case of the FFL, the two remaining field derivatives have a strength of approximately $0.5\,\mathrm{T\,m^{-1}}$ (systems power consumption $P \sim 200\,\mathrm{W}$). Additionally, different FFPs are shown. The first one is a central FFP offering $\sigma_1 = 1.1\,\mathrm{T\,m^{-1}}$, $\sigma_3 = 0.5$ ($P \sim 250\,\mathrm{W}$). The second FFP is shifted by 2 cm towards the coil cages. At this position $\sigma_1 = 1.8\,\mathrm{T\,m^{-1}}$ and $\sigma_3 = 0.7\,\mathrm{T\,m^{-1}}$ is measured in the FFP ($P \sim 270\,\mathrm{W}$). The third FFP is shifted in all directions. Here, $\sigma_1 = 0.8\,\mathrm{T\,m^{-1}}$ and $\sigma_3 = 0.3\,\mathrm{T\,m^{-1}}$ were determined ($P \sim 170\,\mathrm{W}$). No significant temperature rise in the coils has been detected so far in the measurements presented.

IV. Discussion and Conclusion

The presented field generator can generate a variety of magnetic fields that can be used for a wide range of applications. More specifically, it enables the generation of FFPs, FFLs, and other complex shaped fields. Besides the various applications for magnetic actuation, the calculation and generation of certain fields under the influence of nonlinear magnetization response can also be studied. Currently, the fields are still partially limited by the fact that the total current in the system is limited by the maximum current of the used current source. An additional current source and better current calculation algorithms would further enhance the system's capabilities.

Acknowledgments

The authors thankfully acknowledge the financial support by the German Research Foundation (DFG, grant number KN 1108/7-1 and GR 5287/2-1).

Author's statement

Conflict of interest: Authors state no conflict of interest.

References

[1] J. Rahmer, C. Stehning, and B. Gleich. Remote magnetic actuation using a clinical scale system. *PLOS ONE*, 13(3):e0193546, 2018, Publisher: Public Library of Science. doi:10.1371/journal.pone.0193546.

[2] M. Graeser, F. Thieben, P. Szwargulski, F. Werner, N. Gdaniec, M. Boberg, F. Griese, M. Möddel, P. Ludewig, D. van de Ven, O. M. Weber, O. Woywode, B. Gleich, and T. Knopp. Human-sized magnetic particle imaging for brain applications. *Nature Communications*, 10(1):1936, 2019, doi:10.1038/s41467-019-09704-x.

[3] P. Vogel, M. A. Ruckert, P. Klauer, W. H. Kullmann, P. M. Jakob, and V. C. Behr. Traveling Wave Magnetic Particle Imaging. *IEEE Transactions on Medical Imaging*, 33(2):400–407, 2014, doi:10.1109/TMI.2013.2285472.

[4] F. Foerger, M. Graeser, and T. Knopp. Iron core coil designs for MPI. *International Journal on Magnetic Particle Imaging*, pp. Vol 6 No 2 Suppl. 1 (2020), 2020, doi:10.18416/IJMPI.2020.2009042.

[5] K. Sajjamark, J. Franke, H. Lehr, R. Pietig, and V. Niemann. Spatial selectivity enhancement in magnetic fluid hyperthermia by magnetic flux confinement. *International Journal on Magnetic Particle Imaging*, pp. Vol 7 No 1 (2021), 2021, doi:10.18416/IJMPI.2021.2103002.

[6] F. Foerger, M. Boberg, M. Möddel, J.-P. Scheel, M. Graeser, and T. Knopp. Low-Power Iron Selection and Focus Field Generator. *International Journal on Magnetic Particle Imaging*, pp. Vol 8 No 1 Suppl 1 (2022), 2022, doi:10.18416/IJMPI.2022.2203065.

[7] F. Foerger, J.-P. Scheel, F. Thieben, F. Mohn, T. Knopp, and M. Graeser. Multi-Channel Current Control System for Coupled Multi-Coil Arrays. *International Journal on Magnetic Particle Imaging*, pp. Vol 8 No 1 Suppl 1 (2022), 2022, doi:10.18416/IJMPI.2022.2203076.

[8] N. Hackelberg, J. Schumacher, M. Graeser, and T. Knopp. A Flexible High-Performance Signal Generation and Digitization Platform based on Low-Cost Hardware. *International Journal on Magnetic Particle Imaging*, pp. Vol 8 No 1 Suppl 1 (2022), 2022, doi:10.18416/IJMPI.2022.2203063.

[9] N. Hackelberg, J. Schumacher, J. Ackers, M. Möddel, F. Foerger, M. Graeser, and T. Knopp. MPIMeasurements.jl: An Extensible Julia Framework for Composable Magnetic Particle Imaging Devices. *International Journal on Magnetic Particle Imaging*, 9(1 Suppl 1), 2023.

[10] M. Boberg, T. Knopp, and M. Möddel. Analysis and Comparison of Magnetic Fields in MPI using Spherical Harmonic Expansions. *8th International Workshop on Magnetic Particle Imaging (IWMPI 2018)*, pp. 159–160, 2018.